

Evolutionary status of Polaris

Yu. A. Fadeyev^{*}

Institute of Astronomy of the Russian Academy of Sciences, 48 Pyatnitskaya St., 119017, Moscow, Russia

Accepted 2015 February 23. Received 2015 February 21; in original form 2015 February 1

ABSTRACT

Hydrodynamic models of short-period Cepheids were computed to determine the pulsation period as a function of evolutionary time during the first and third crossings of the instability strip. The equations of radiation hydrodynamics and turbulent convection for radial stellar pulsations were solved with the initial conditions obtained from the evolutionary models of population I stars ($X = 0.7$, $Z = 0.02$) with masses from $5.2M_{\odot}$ to $6.5M_{\odot}$ and the convective core overshooting parameter $0.1 \leq \alpha_{\text{ov}} \leq 0.3$. In Cepheids with period of 4 d the rate of pulsation period change during the first crossing of the instability strip is over fifty times larger than that during the third crossing. Polaris is shown to cross the instability strip for the first time and to be the fundamental mode pulsator. The best agreement between the predicted and observed rates of period change was obtained for the model with mass of $5.4M_{\odot}$ and the overshooting parameter $\alpha_{\text{ov}} = 0.25$. The bolometric luminosity and radius are $L = 1.26 \cdot 10^3 L_{\odot}$ and $R = 37.5 R_{\odot}$, respectively. In the HR diagram Polaris is located at the red edge of the instability strip.

Key words: stars: evolution – stars: fundamental parameters – stars: individual: α UMi (Polaris) – stars: variables: Cepheids

1 INTRODUCTION

Polaris (α UMi) is a short-period ($\Pi \approx 3.969$ d) small-amplitude Cepheid with steadily increasing pulsation period (Ferne 1966; Arellano Ferro 1983; Dinshaw et al. 1989). The rate of period change is estimated from $\dot{\Pi} = 4.5 \text{ s yr}^{-1}$ (Turner et al. 2005) to $\dot{\Pi} = 4.9 \text{ s yr}^{-1}$ (Spreckley & Stevens 2008). These values are over an order of magnitude larger than the rates of period change in most of the Cepheids with a period of $\Pi \approx 4$ d. This lead Berdnikov et al. (1997) to the conclusion that Polaris is undergoing the first crossing of the instability strip after the main-sequence phase. Neilson et al. (2012) and Neilson (2014) however casted doubts on this assumption and argued that Polaris is evolving along the blue loop. They also showed that the observed rate of period change is more consistent with predictions from stellar evolution models provided that Polaris is currently loosing mass at a rate of $\dot{M} \sim 10^{-6} M_{\odot} \text{ yr}^{-1}$.

Since about the middle twentieth century Polaris showed decrease in photometric and radial velocity amplitudes (Arellano Ferro 1983; Ferne et al. 1993). Dinshaw et al. (1989) supposed that Polaris is approaching the red edge of the instability strip but in 1994–1997 the decrease in amplitude has stopped (Kamper & Ferne 1998). Recent photometric and radial velocity measurements reveal slow increase of the pulsation amplitude (Bruntt et al. 2008;

Lee et al. 2008; Spreckley & Stevens 2008). The cause of the amplitude growth remains unknown. Ferne et al. (1993), Evans et al. (2002), Turner et al. (2005) reported that Polaris lies well inside the instability strip.

Polaris is the nearest Cepheid and determination of its pulsation mode is of great importance in establishing the Cepheid period–luminosity relation. Feast & Catchpole (1997) showed that the *Hipparcos* trigonometrical parallax data are consistent with first overtone pulsation in Polaris. This conclusion was later confirmed by nonlinear stellar pulsation models by Bono et al. (2001). However recent measurements of photometric and spectroscopic parallaxes seem to be more consistent with fundamental mode pulsation (Turner et al. 2013).

The *Hipparcos* parallax of 7.54 ± 0.11 mas (van Leeuwen 2007) implies a distance to Polaris of $d = 133 \pm 2$ pc but the spectroscopic and photometric parallaxes give the distance from $d = 99 \pm 2$ pc (Turner et al. 2013) to $d = 110$ pc (Usenko & Klochkova 2008). Therefore the mean angular diameter of 3.28 mas measured with the Navy Prototype Optical Interferometer (Nordgren et al. 2000) corresponds to the linear radius of $R = 47 R_{\odot}$ for the distance $d = 133$ pc and $R = 35 R_{\odot}$ for $d = 99$ pc.

Polaris is the primary component of a close binary system with an orbital period of 29.6 yr. Evans et al. (2008) directly detected the secondary component using UV images ($\lambda \sim 2255 \text{ \AA}$) obtained with the Hubble Space Telescope and found that Polaris has a mass in the range $M = 3.1 -$

^{*} E-mail: fadeyev@inasan.ru

$6.7M_{\odot}$. This is the first direct estimate of the Cepheid dynamical mass.

In this work, we aim to clarify some contradictions mentioned above. We calculate the rates of period change in Cepheids with periods near 4 d and determine the evolutionary status of Polaris by comparing the observed rate with theoretical predictions. To this end we compute the non-linear stellar pulsation models as solution of the equations of radiation hydrodynamics and turbulent convection with initial conditions obtained from the evolutionary computations. Such an approach the author used earlier to obtain theoretical rates of pulsation period change in LMC and Galactic Cepheids (Fadeyev 2013, 2014). In comparison with previous works both evolutionary and hydrodynamical computations of this study were carried out with improved input physics. As shown below, determination of the evolutionary status provides constraints on the pulsation mode and the fundamental parameters of Polaris.

2 METHODS OF COMPUTATION

2.1 Stellar evolution

This work is aimed at determining the pulsation period Π as a function of evolutionary time t_{ev} during the first and third crossings of the Cepheid instability strip. We computed the evolutionary tracks for non-rotating population I stars with initial masses $5.2M_{\odot} \leq M_{\text{ZAMS}} \leq 6.5M_{\odot}$ evolving from the zero age main sequence (ZAMS) until the end of core helium burning. Initial mass fractional abundances of hydrogen and heavy elements are $X = 0.7$ and $Z = 0.02$, respectively. The initial relative abundances of the elements heavier than helium normalized by Z were determined according to Asplund et al. (2009). Evolutionary computations were done with a code implementing the Henyey method (Fadeyev 2007, 2010). Below we comment some improvements used in the present work.

Thermodynamic quantities are obtained by interpolation in the tables calculated with the library of programs FreeEOS (Irwin 2012). Rosseland opacities are computed from OPAL data (Iglesias & Rogers 1996) complemented at low temperatures by the opacities from (Ferguson et al. 2005). The nuclear reaction rates are from the NACRE database (Angulo et al. 1999) with updates for reactions $^{14}\text{N}(p,\gamma)^{15}\text{O}$, $^4\text{He}(\alpha,\alpha,\gamma)^{12}\text{C}$ and $^{12}\text{C}(\alpha,\gamma)^{16}\text{O}$ that were taken from the REACLIB database (Rauscher et al. 2010).

In the evolutionary computations convection is treated according to the mixing length theory (Böhm-Vitense 1958) using a mixing-length parameter $\alpha_{\Lambda} = 1.6$. Boundaries of convective zones are determined with the Schwarzschild criterion but the convective core is extended in radius by $\alpha_{\text{ov}}H_{\text{P}}$, where H_{P} is the pressure scale height and α_{ov} is the dimensionless overshooting parameter ranging from 0.1 to 0.3.

To assure the gradual growth of the convective core during the core helium burning phase the evolutionary models were computed with $\sim 10^4$ mass zones. The mass loss rate \dot{M} during the main sequence phase is from formulae by Vink et al. (1999, 2000, 2001) and outside their domain \dot{M} is evaluated according to Nieuwenhuijzen & de Jager (1990). It should be noted that in our problem the role

of mass loss is insignificant. For example, the mass of the Cepheid $M_{\text{ZAMS}} = 5.9M_{\odot}$ during the first and third crossings of the instability strip is $M = 5.89M_{\odot}$ and $M = 5.84M_{\odot}$, respectively.

Bearing in mind the importance of initial conditions for correct determination of the predicted rates of pulsation period change we carried out additional evolutionary computations for stars with initial composition $X = 0.72$, $Z = 0.014$ and the overshooting parameter $\alpha_{\text{ov}} = 0.1$. Results of these computations were compared with evolutionary models of non-rotating stars with initial masses $5M_{\odot}$ and $7M_{\odot}$ (Ekström et al. 2012). The difference in luminosity and time scales was found to be less than 5 per cent.

2.2 Non-linear stellar pulsation

To compute non-linear stellar pulsation models we solve the Cauchy problem for the equations of one-dimensional radiation hydrodynamics with time-dependent turbulent convection treated according to Kuhfuß (1986). The equations are written as

$$\frac{dU}{dt} = -\frac{GM_r}{r^2} - \frac{1}{\rho} \frac{\partial}{\partial r} (P + P_t) + \dot{U}_{\text{tv}}, \quad (1)$$

$$\frac{dE}{dt} + P \frac{dV}{dt} = -\frac{1}{\rho r^2} \frac{\partial}{\partial r} [r^2 (F_r + F_c)] - C_t, \quad (2)$$

$$\frac{dE_t}{dt} + P_t \frac{dV}{dt} = -\frac{1}{\rho r^2} \frac{\partial}{\partial r} (r^2 F_t) + C_t + \dot{E}_{\text{tv}}. \quad (3)$$

Here t is time, G is the Newtonian constant of gravitation, M_r is the mass interior to radius r , U is the velocity of the gas flow, P is the total (gas plus radiation) pressure, ρ is gas density and $V = 1/\rho$ is specific volume, E is the specific internal energy of gas, F_r is the radiation flux computed in the diffusion approximation. The turbulent pressure P_t is related to the specific turbulent kinetic energy E_t by $P_t = \frac{2}{3}\rho E_t$.

The convective flux is

$$F_c = \rho T \Pi, \quad (4)$$

where T is the gas temperature,

$$\Pi = -\alpha_{\Lambda} \alpha_s H_{\text{P}} E_t^{1/2} \frac{\partial S}{\partial r} = \alpha_{\Lambda} \alpha_s E_t^{1/2} C_{\text{P}} (\nabla - \nabla_{\text{a}}) \quad (5)$$

is the correlation between entropy and velocity fluctuations, $\nabla = d \ln T / d \ln P$, $\nabla_{\text{a}} = (\partial \ln T / \partial \ln P)_{\text{S}}$, C_{P} is the specific heat at constant pressure, S is the specific entropy.

The turbulent kinetic energy flux is

$$F_t = -\alpha_{\Lambda} \alpha_t \rho H_{\text{P}} E_t^{1/2} \frac{\partial E_t}{\partial r}. \quad (6)$$

The coupling term is

$$C_t = S_t - D_t - D_r, \quad (7)$$

where

$$S_t = \frac{T}{H_{\text{P}}} \nabla_{\text{a}} \Pi \quad (8)$$

is the source of specific turbulent energy due to buoyancy forces,

$$D_t = \frac{\alpha_{\text{d}}}{\alpha_{\Lambda}} \frac{E_t^{3/2}}{H_{\text{P}}} \quad (9)$$

is the dissipation of specific turbulent energy due to molecular viscosity. The radiative dissipation is

$$D_r = \frac{E_t}{\tau_{\text{rad}}}, \quad (10)$$

where

$$\tau_{\text{rad}} = \frac{\alpha_\Lambda^2}{\gamma_{\text{rad}}^2} \frac{C_P \kappa P^2}{4\sigma g^2 T^3}, \quad (11)$$

σ is the Stefan–Boltzmann constant, κ is opacity, $g = GM_r/r^2$ is the gravitational acceleration.

Viscous momentum and energy transfer rates are

$$\dot{U}_{\text{tv}} = \frac{1}{r^3 \rho} \frac{\partial}{\partial r} \left[\frac{4}{3} \mu_{\text{tv}} r^3 \left(\frac{\partial U}{\partial r} - \frac{U}{r} \right) \right] \quad (12)$$

and

$$\dot{E}_{\text{tv}} = \frac{4}{3} \frac{\mu_{\text{tv}}}{\rho} \left(\frac{\partial U}{\partial r} - \frac{U}{r} \right)^2, \quad (13)$$

respectively, where

$$\mu_{\text{tv}} = \alpha_\Lambda \alpha_m \rho H_P E_t^{1/2} \quad (14)$$

is the kinetic turbulent viscosity.

Formulae (5), (6), (9), (11) and (14) contain dimensionless parameters α_Λ , α_s , α_t , α_d , γ_{rad} and α_m . The mixing length to pressure scale height ratio is the same as in the evolutionary computations: $\alpha_\Lambda = 1.6$. Parameters α_s , α_t , and α_d are set according to Wuchterl & Feuchtinger (1998):

$$\alpha_s = \frac{1}{2} \sqrt{\frac{2}{3}}, \quad \alpha_t = 0.6093 \alpha_s, \quad \alpha_d = \frac{8}{3} \sqrt{\frac{2}{3}}.$$

Appropriate values $\gamma_{\text{rad}} = 0.4\sqrt{3}$ and $\alpha_m = 0.1$ were determined from trial computations of Cepheid models (Fadeyev 2014). Thus, the parameter γ_{rad} in the expression for the radiative cooling time of convective elements (11) is five times smaller than originally proposed by Wuchterl & Feuchtinger (1998). It should be noted that nearly the same parameters were found to be most appropriate for Cepheid modelling in works by Kolláth et al. (2002), Szabó et al. (2007), Smolec & Moskalik (2008, 2010).

In our study we consider the self-excited radial oscillations. The initial hydrodynamic model is computed by interpolating the zonal quantities of the evolutionary model and interpolation errors play the role of small initial perturbations. To diminish the amplitude of initial perturbations we used fine zoning in mass in the outer layers of the evolutionary model so that as many as $3 \cdot 10^3$ outer mass zones had the relative radius $r > 0.1R$, where R is the radius of the star. All hydrodynamic models were computed for $N = 500$ mass zones. The mass intervals increase geometrically inward with the ratio of $q \approx 1.03$. The radius r_1 and luminosity L_1 at the innermost zone are assumed to be time-independent. The radius of the inner boundary satisfies the condition $r_1 \leq 0.1R$.

3 RATES OF PULSATION PERIOD CHANGE

Together with numerical integration of equations (1) – (3) with respect to time t we calculate the kinetic energy

$$E_K(t) = \frac{1}{2} \sum_{j=2}^N \Delta M_{j-1/2} U_j(t)^2, \quad (15)$$

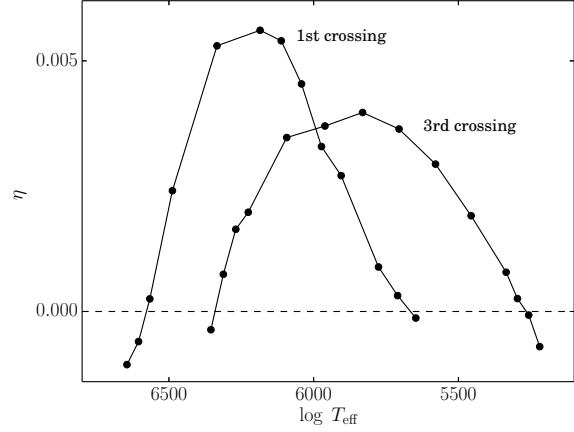


Figure 1. The pulsation growth rate η as a function of effective temperature T_{eff} during the first and third crossings of the instability strip for the evolutionary sequence $M_{\text{ZAMS}} = 5.9M_\odot$, $\alpha_{\text{ov}} = 0.1$. Hydrodynamic models are shown by filled circles.

where $\Delta M_{j-1/2} = M_j - M_{j-1}$ and M_j is the Lagrangian coordinate of the j -th mass zone. The kinetic energy reaches the maximum value $E_{K,\text{max}}$ twice per pulsation period Π and for the initial interval of integration with exponential change of $E_{K,\text{max}}$ we evaluate the pulsation growth rate $\eta = \Pi d \ln E_{K,\text{max}} / dt$. The period Π is determined by a discrete Fourier transform of $E_K(t)$. The total sampling interval ranges from 10^3 to 10^4 pulsation cycles.

Fig. 1 shows the pulsation growth rate η as a function of effective temperature T_{eff} during the first and third crossings of the instability strip for hydrodynamic models of the evolutionary sequence $M_{\text{ZAMS}} = 5.9M_\odot$, $\alpha_{\text{ov}} = 0.1$. The evolutionary time t_{ev} , stellar luminosity L and stellar radius R at the edges of the instability strip are determined for $\eta = 0$ by linear interpolation between two adjacent hydrodynamic models with growth rates of opposite signs. The time spent in the instability strip is $\Delta t_{\text{ev},1} = 1.60 \cdot 10^4$ yr during the first crossing and $\Delta t_{\text{ev},3} = 4.26 \cdot 10^5$ yr during the third crossing. The ratio $\Delta t_{\text{ev},3} / \Delta t_{\text{ev},1}$ increases with mass and ranges from 25 to 30 for $5.6M_\odot \leq M_{\text{ZAMS}} \leq 6.1M_\odot$.

Evolutionary tracks for stars with initial masses $5.6M_\odot$ and $5.9M_\odot$ ($\alpha_{\text{ov}} = 0.1$) are displayed in Fig. 2. The sections of the evolutionary tracks corresponding to pulsations with increasing period (the first and third crossings of the instability strip) are shown by dotted lines. Cepheids with decreasing periods are beyond the scope of the present study and therefore the second crossing of the instability strip is not indicated in the plots.

The upper panel of Fig. 3 shows the temporal dependence of the pulsation period Π during the first crossing of the instability strip for the evolutionary sequence $M_{\text{ZAMS}} = 5.9M_\odot$, $\alpha_{\text{ov}} = 0.1$. For the sake of convenience we use $\tau = t_{\text{ev}} - t_{\text{ev,b}}$ as an independent variable, where $t_{\text{ev,b}}$ is the evolutionary time at the blue edge of the instability strip. Periods of pulsationally stable and pulsationally unstable models are shown by open circles and filled circles, respectively.

During the first crossing of the instability strip the star begins to pulsate in the first overtone but as the star ap-

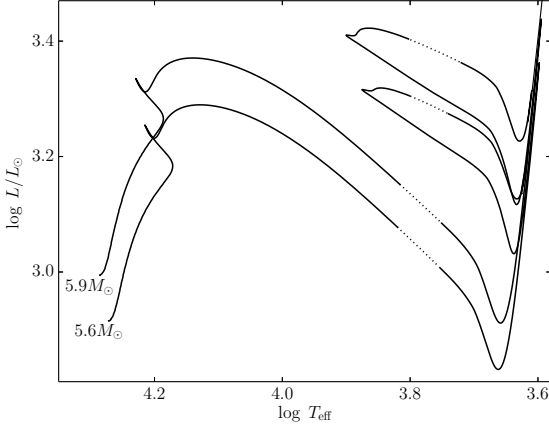


Figure 2. Evolutionary tracks of stars $M_{\text{ZAMS}} = 5.6 M_{\odot}$ and $M_{\text{ZAMS}} = 5.9 M_{\odot}$ ($\alpha_{\text{ov}} = 0.1$). The sections of tracks corresponding to the first and third crossings of the instability strip are indicated by dotted lines.

proaches the red edge it becomes the fundamental-mode pulsator. For hydrodynamic models near the pulsational mode switching we evaluated the periods of the first overtone (1h) and fundamental mode (f) using the additional discrete Fourier transform of E_K . The sampling interval was limited by the amplitude growth stage when the power spectrum reveals the presence of secondary modes with decaying amplitudes. Periods of such modes are shown in the upper panel of Fig. 3 by open triangles. The boundary between the first overtone and fundamental mode pulsators is defined as a middle point between two adjacent hydrodynamic models with different orders of the primary mode. For the first crossing of the instability strip the second-order algebraic polynomials approximate the temporal dependence $\Pi(\tau)$ with an rms error less than 0.1%. In the upper panel of Fig. 3 the analytical fits are shown by solid lines.

Time derivatives of analytical fits to $\Pi(\tau)$ are shown in the lower panel of Fig. 3 as a function of pulsation period Π . For the sake of convenience the rate of pulsation period change $\dot{\Pi}$ is expressed in units of seconds per year. Solid squares show estimates of $\dot{\Pi}$ obtained by numerical differentiation. The small deviation of numerical derivatives from the analytical fits to $\dot{\Pi}(\tau)$ is due to the limited accuracy of evolutionary calculations.

Fig. 4 displays the temporal dependence of Π (upper panel) and the plot of $\dot{\Pi}$ as a function of Π (lower panel) for models of the evolutionary sequence $M_{\text{ZAMS}} = 5.9 M_{\odot}$, $\alpha_{\text{ov}} = 0.1$ during the third crossing of the instability strip. All hydrodynamic models were found to pulsate in the fundamental mode. The temporal dependence $\Pi(\tau)$ is fitted with the relative rms error less than 0.1% by the fourth-order algebraic polynomial.

The results of polynomial fitting for hydrodynamic models with pulsation periods $2 \text{ d} \leq \Pi \leq 8 \text{ d}$ are displayed in Fig. 5 where the rates of period change $\dot{\Pi}$ are plotted as a function of period Π for evolutionary sequences with initial masses $5.4 M_{\odot} \leq M_{\text{ZAMS}} \leq 5.9 M_{\odot}$ and the overshooting parameter $\alpha_{\text{ov}} = 0.1$. Each curve in this diagram describes the evolution of values Π , $\dot{\Pi}$ as the star crosses the instability

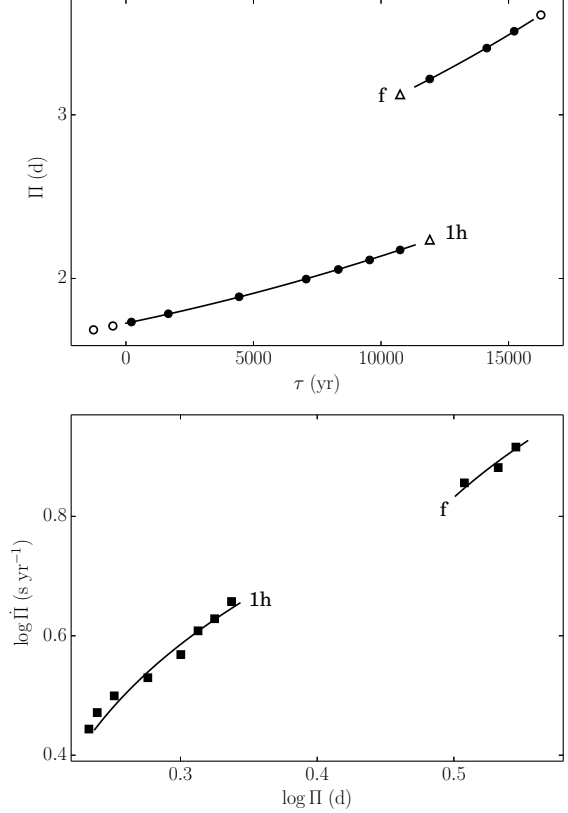


Figure 3. The pulsation period Π as a function of evolutionary time τ (upper panel) and the rate of period change $\dot{\Pi}$ as a function of period Π (lower panel) during the first crossing of the instability strip for the evolutionary sequence $M_{\text{ZAMS}} = 5.9 M_{\odot}$, $\alpha_{\text{ov}} = 0.1$. In the upper panel solid lines show the second-order polynomial fits, open circles and filled circles show the periods of pulsationally stable and pulsationally unstable models, respectively. Open triangles show the periods of the secondary mode near the mode switching. In the lower panel solid lines show time derivatives of analytical fits. Solid squares represent the time derivatives obtained by numerical differentiation.

strip. The solid and dashed lines represent the fundamental mode and first overtone, respectively. The plots located in the upper part of Fig. 5 represent the first crossing of the instability strip and the plots located in the lower part of the diagram correspond to the third crossing. As is clearly seen, for Cepheids with a period of $\Pi \approx 4 \text{ d}$ the rate of period change during the first crossing of the instability strip $\dot{\Pi}_1$ is over fifty times larger than the rate of period change during the third crossing $\dot{\Pi}_3$. It should be noted that large values of the ratio $\dot{\Pi}_1/\dot{\Pi}_3$ are also typical for long-period Cepheids (Fadeyev 2014).

The position of Polaris is marked in Fig. 5 for the period $\Pi_* = 3.969 \text{ d}$ and the rate of period change $\dot{\Pi}_* = 4.7 \text{ s yr}^{-1}$ which is the mean value of the observational estimates by Turner et al. (2005) and Spreckley & Stevens (2008). Even a cursory glance at Fig. 5 leads us to the following conclusions: (1) Polaris crosses the instability strip for the first time; (2)

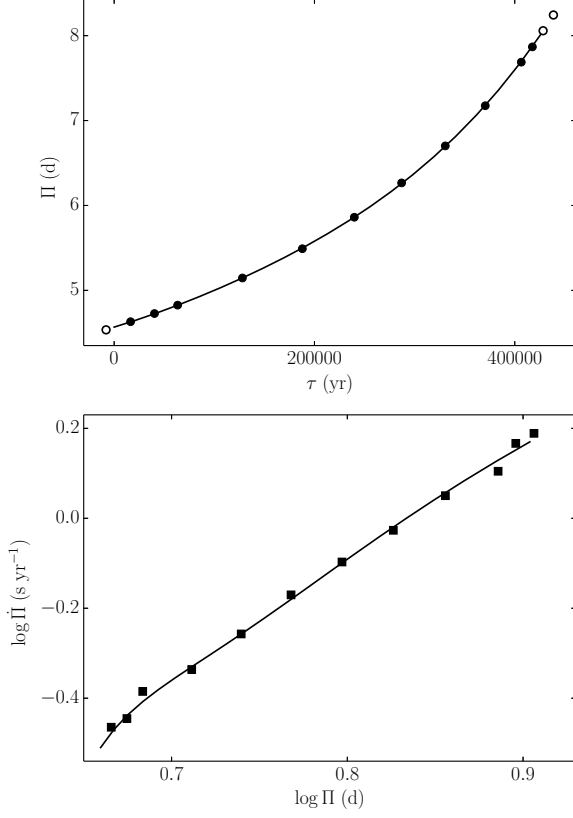


Figure 4. Same as Fig. 3, but for the third crossing of the instability strip. All hydrodynamic models show pulsations in the fundamental mode. The solid lines represent the fourth-order polynomial fitting (upper panel) and its time derivative (lower panel).

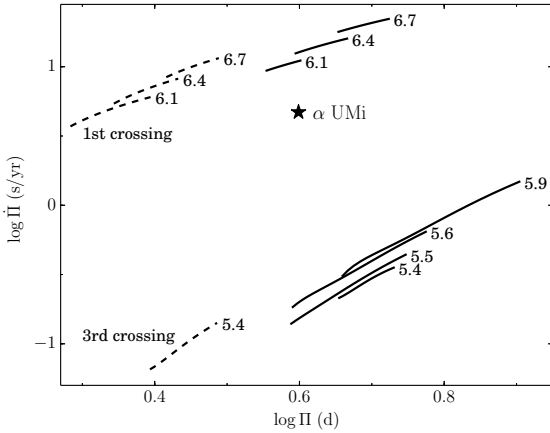


Figure 5. The rate of period change $\dot{\Pi}$ as a function of pulsation period Π for evolutionary sequences with $\alpha_{ov} = 0.1$ during the first and third crossings of the instability strip. The numbers at the curves indicate the initial stellar mass M_{ZAMS} in solar units. Solid and dashed lines correspond to the fundamental mode and first overtone, respectively.

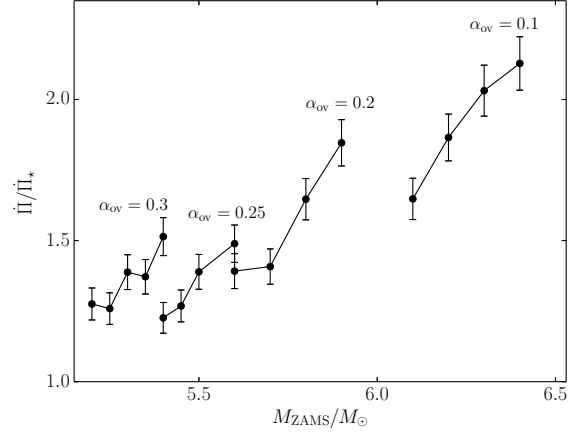


Figure 6. The ratio of the predicted to observed rates of period change $\dot{\Pi}/\dot{\Pi}_*$ as a function of initial stellar mass M_{ZAMS} for the overshooting parameters $\alpha_{ov} = 0.1, 0.2, 0.25$ and 0.3 .

Polaris is the fundamental mode pulsator. Below we discuss in more detail both these conclusions.

The diagram in Fig. 5 was obtained for the evolutionary sequences computed with the overshooting parameter $\alpha_{ov} = 0.1$ and the ratio of the predicted to observed rates of period change is $\dot{\Pi}/\dot{\Pi}_* \approx 2$. However the rate of period change during the first crossing of the instability strip depends on the assumed overshooting during the main-sequence evolutionary phase, so that agreement between theory and observations can be substantially improved. This is illustrated by Fig. 6 where the ratio $\dot{\Pi}/\dot{\Pi}_*$ is plotted as a function of initial mass M_{ZAMS} for several values of the overshooting parameter α_{ov} . The upper and lower errorbars correspond to the observational estimates by Turner et al. (2005) and Sreckley & Stevens (2008), respectively. As seen from Fig. 6, the best agreement between the predicted and observed rates of period change ($\dot{\Pi}/\dot{\Pi}_* \approx 1.25$) is obtained for the overshooting parameter $\alpha_{ov} = 0.25$ and the initial stellar mass $5.4M_{\odot} \leq M_{ZAMS} \leq 5.45M_{\odot}$.

4 FUNDAMENTAL PARAMETERS OF POLARIS

To determine the pulsation mode of first-crossing Cepheids with period of $\Pi = 3.969$ d we considered the grid of evolutionary and hydrodynamic models with initial stellar masses $5.2M_{\odot} \leq M_{ZAMS} \leq 6.5M_{\odot}$ and the overshooting parameter ranging from 0.1 to 0.3. Typical results obtained for the overshooting parameter $\alpha_{ov} = 0.2$ are shown in Fig. 7.

The filled circles connected by dashed lines in Fig. 7 show the pulsation period at the blue and red edges of the instability strip, whereas the open circles connected by dotted lines show the pulsation period at the mode switch. Thus, for a fixed value of M_{ZAMS} the plots in Fig. 7 show the range of periods for pulsations in the first overtone and in the fundamental mode. The similar diagrams were obtained for other values of the overshooting parameter α_{ov} and no models pulsating in the first overtone with period of $\Pi = 3.969$ d were found. Therefore, Polaris is undoubtedly a fundamental-mode pulsator.

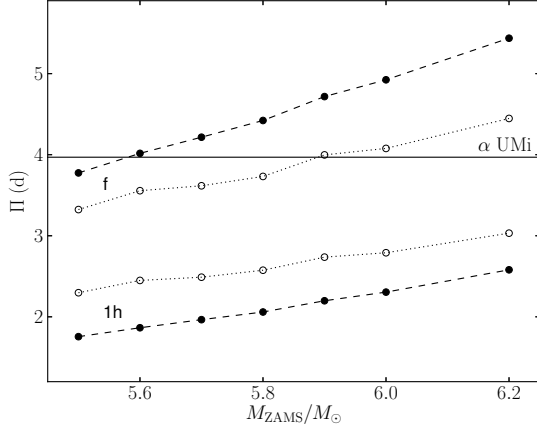


Figure 7. The pulsation period at the blue edge (lower dashed line) and red edge (upper dashed line) of the instability strip for models of first-crossing Cepheids computed with the overshooting parameter $\alpha_{ov} = 0.2$. Lower and upper dotted lines show the periods of the first overtone and fundamental mode at the mode switch boundary. Filled and open circles represent the interpolated values of the period.

Table 1. The upper and lower values of the fundamental parameters of Polaris

α_{ov}	M/M_{\odot}	L/L_{\odot}	R/R_{\odot}	T_{eff} (K)	d (pc)
0.1	6.38	1770	39.9	5930	113
	6.08	1390	39.3	5630	111
0.2	5.88	1660	38.7	5930	110
	5.59	1300	37.8	5640	107
0.25	5.59	1510	37.9	5850	107
	5.39	1260	37.4	5640	106
0.3	5.39	1450	37.5	5820	106
	5.19	1220	36.7	5630	104

Intersection of the dashed and dotted lines with the solid horizontal line $\Pi = 3.969$ d in Fig. 7 gives the lower and upper values for the initial stellar mass M_{ZAMS} , respectively. The upper and lower values of the mass M , radius R and luminosity L are evaluated by interpolation between the evolutionary tracks.

Fig. 8 shows the evolutionary tracks in the HR diagram for stars with initial masses $5.5M_{\odot}$ and $6.2M_{\odot}$ ($\alpha_{ov} = 0.2$). The dashed lines show the blue and red edges of the instability strip. The mode switch boundary shown by the dotted line is not the straight line due to difficulties in determining the exact location of the point of mode switch. Models with pulsation period $\Pi_{\star} = 3.969$ day are shown by the star symbol.

The lower and upper values of fundamental parameters for Polaris are given in Table 1. The last column gives the distance to Polaris d evaluated from the observed angular diameter $\theta_L = 3.28$ mas (Nordgren et al. 2000).

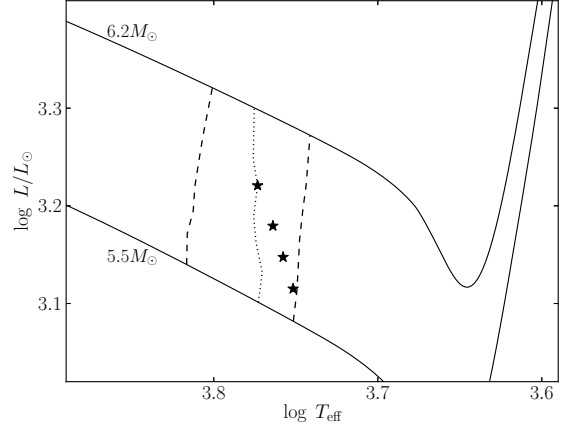


Figure 8. Evolutionary tracks of stars with initial masses $5.5M_{\odot}$ and $6.2M_{\odot}$ ($\alpha_{ov} = 0.2$) near the first crossing of the instability strip. Dashed lines show the blue and red edges of the instability strip. The dotted line shows the mode switch boundary. The star symbols show the location of models with the pulsation period $\Pi_{\star} = 3.969$ day.

5 CONCLUSION

The evolutionary and pulsational models together with the observed period Π_{\star} allow us to obtain the lower and upper estimates of the initial mass of Polaris. As seen in Fig. 6 a major cause of uncertainty in the determination of mass is the overshooting parameter α_{ov} which is the unknown a priori quantity. The comparison of theoretical predictions with the observed rate of period increase leads to the narrower mass range $5.2M_{\odot} \leq M_{ZAMS} \leq 5.7M_{\odot}$ and to the constraint on the overshooting parameter $\alpha_{ov} \geq 0.2$. The best agreement with observations ($\dot{\Pi}/\Pi_{\star} \approx 1.25$) was found for the model $M_{ZAMS} = 5.4M_{\odot}$, $\alpha_{ov} = 0.25$ which locates near the red edge of the instability strip. The mass, $M = 5.39M_{\odot}$, is within the range $3.1M_{\odot} \leq M \leq 6.7M_{\odot}$ of the measured dynamical mass (Evans et al. 2008).

The mean linear radius $R = 37.5 R_{\odot}$ for the overshooting parameter $\alpha_{ov} = 0.25$ (see Table 1) and the observed angular diameter $\theta_L = 3.28$ mas (Nordgren et al. 2000) lead to the distance of $d = 106$ pc. This value is consistent with photometric and spectroscopic parallaxes implying a distance from 99 pc (Turner et al. 2013) to 110 pc (Usenko & Klochkova 2008). To further improve theoretical predictions one has to take into account effects of initial chemical composition. For example, preliminary computations showed that the increase of the fractional mass abundance of hydrogen from $X = 0.7$ to $X = 0.73$ leads to decrease in $\dot{\Pi}$ by $\approx 12\%$.

The fact that Polaris is evolving on a Kelvin–Helmholtz timescale after the main sequence phase and is crossing the instability strip for the first time allows us to conclude that effects of mass loss do not play a significant role in evolutionary changes of the pulsation period.

Decrease of the ratio $\dot{\Pi}/\Pi_{\star}$ with decreasing initial mass M_{ZAMS} at the fixed value of the overshooting parameter favours the closer location of Polaris to the red edge of the instability strip. This assumption does not necessarily contradict the growth of the pulsation amplitude observed

for two last decades. Indeed, the balance between the κ -mechanism exciting pulsational instability and convection which suppresses oscillations can cyclically change due to variations of magnetic field on time scale longer than the pulsation period. Therefore, the currently observed increase of the pulsation amplitude might be due to the growth of a magnetic field which tends to weaken convection (Stothers 2009). Longitudinal magnetic fields from 10 to 30 Gauss were detected in Polaris by (Borra et al. 1981), whereas Usenko et al. (2010) reported on detection of variable magnetic field from -109 to 162 Gauss.

The present study is based on the convection model by Kuhfuß (1986) which contain several parameters of order unity. The most uncertain of them are γ_{rad} and α_m in expressions for the radiative cooling time (11) and kinetic turbulent viscosity (14), respectively. The values of these parameters affect the damping of oscillations and are inferred from observational constraints (for example, the width of the instability strip). At the same time, the uncertainty in the values of γ_{rad} and α_m does not play an important role in determining the pulsation period. This is due to the fact that the depth of the convective zone in Cepheids is only a few per cent of the stellar radius, whereas the length of the fundamental mode period is of the order of two sound travel times between the centre and the surface of the star.

REFERENCES

- Angulo C., Arnould M., Rayet M., Descouvemont P., Baye D., Leclercq-Willain C., Coc A., Barhoumi S., Aguer P., Rolfs C., Kunz R., Hammer J. W., Mayer A., Paradellis T., Kossionides S., Chronidou C., Spyrou K., Degl'Innocenti S., Fiorentini G., Ricci B., Zavatarelli S., Providencia C., Wolters H., Soares J., Grama C., Rahighi J., Shotton A., Laméhi Rachti M., 1999, *Nucl. Phys. A*, 656, 3
- Arellano Ferro A., 1983, *ApJ*, 274, 755
- Asplund M., Grevesse N., Sauval A. J., Scott P., 2009, *ARA&A*, 47, 481
- Berdnikov L. N., Ignatova V. V., Pastukhova E. N., Turner D. G., 1997, *Astron. Lett.*, 23, 177
- Böhm-Vitense E., 1958, *ZA*, 46, 108
- Bono G., Gieren W. P., Marconi M., Fouqué P., 2001, *ApJ*, 552, L141
- Borra E. F., Fletcher J. M., Poeckert R., 1981, *ApJ*, 247, 569
- Bruntt H., Evans N. R., Stello D., Penny A. J., Eaton J. A., Buzasi D. L., Sasselov D. D., Preston H. L., Miller-Ricci E., 2008, *ApJ*, 683, 433
- Ekström S., Georgy C., Eggenberger P., Meynet G., Mowlavi N., Wyttenbach A., Granada A., Decressin T., Hirschi R., Frischknecht U., Charbonnel C., Maeder A., 2012, *A&A*, 537, A146
- Evans N. R., Sasselov D. D., Short C. I., 2002, *ApJ*, 567, 1121
- Evans N. R., Schaefer G. H., Bond H. E., Bono G., Karovska M., Nelan E., Sasselov D., Mason B. D., 2008, *AJ*, 136, 1137
- Fadeyev Yu. A., 2007, *Astron. Lett.*, 33, 692
- Fadeyev Yu. A., 2010, *Astron. Lett.*, 36, 362
- Fadeyev Yu. A., 2013, *Astron. Lett.*, 39, 746
- Fadeyev Yu. A., 2014, *Astron. Lett.*, 40, 301
- Feast M. W., Catchpole R. M., 1997, *MNRAS*, 286, L1
- Ferguson J. W., Alexander D. R., Allard F., Barman T., Bodnarik J. G., Hauschildt P. H., Heffner-Wong A., Tamanai A., 2005, *ApJ*, 623, 585
- Fernie J. D., 1966, *AJ*, 71, 732
- Fernie J. D., Kamper K. W., Seager S., 1993, *ApJ*, 416, 820
- Dinshaw N., Matthews J. M., Walker G. A. H., Hill G. M., 1989, *AJ*, 98, 2249
- Irwin A. W., FreeEOS: Equation of State for stellar interiors calculations, astrophysics Source Code Library
- Iglesias C. A., Rogers F. J., 1996, *ApJ*, 464, 943
- Kamper K. W., Fernie J. D., 1998, *AJ*, 116, 936
- Kolláth Z., Buchler J. R., Szabó R., Csabry Z., 2002, *A&A*, 385, 932
- Kuhfuß R., 1986, *A&A*, 160, 116
- Lee B.-C., Mkrtichian D. E., Han I., Park M.-G., Kim K.-M., 2008, *AJ*, 135, 2240
- Neilson H. R., 2014, *A&A*, 563, A48
- Neilson H. R., Engle S. G., Guinan E., Langer N., Wasatonic R. P., Williams D. B., 2012, *ApJ*, 745, L32
- Nieuwenhuijzen H., de Jager C., 1990, *A&A*, 231, 134
- Nordgren T. E., Armstrong J. T., Germain M. E., Hindsley R. B., Hajian A. R., Sudol J. J., Hummel C. A., 2000, *ApJ*, 543, 972
- Rauscher T., Sakharuk A., Schatz H., Thielemann F. K., Wiescher M., 2010, *ApJS*, 189, 240
- Smolec R., Moskalik P., 2008, *Acta Astron.*, 58, 193
- Smolec R., Moskalik P., 2010, *A&A*, 524, A40
- Spreckley S. A., Stevens I. R., 2008, *MNRAS*, 388, 1239
- Stothers R. B., 2009, *ApJ*, 696, L37
- Szabó R., Buchler J. R., Bartee J., 2007, *ApJ*, 667, 1150
- Turner D. G., Savoy J., Derrah J., Abdel-Sabour Abdel-Latif M., Berdnikov L. N., 2005, *PASP*, 117, 207
- Turner D. G., Kovtyukh V. V., Usenko I. A., Gorlova, N. I., 2013, *ApJ*, 762, L8
- Usenko I. A., Klochkova V. G., 2008, *MNRAS*, 387, L1
- Usenko I. A., Bychkov V. D., Bychkova L. V., Plachinda S. N., 2010, *OAP*, 23, 140
- van Leeuwen F., 2007, *A&A*, 474, 653
- Vink J. S., de Koter A., Lamers H. J. G. L. M., 1999, *A&A*, 350, 181
- Vink J. S., de Koter A., Lamers H. J. G. L. M., 2000, *A&A*, 362, 295
- Vink J. S., de Koter A., Lamers H. J. G. L. M., 2001, *A&A*, 369, 574
- Wuchterl G., Feuchtinger M. U., 1998, *A&A*, 340, 419